Generation of Fast Ions by Microclusters

Alexey AREFIEV[1)], Boris BREIZMAN[1)], Vladimir KHUDIK[1)], Xiaohui GAO[2)] and Michael DOWNER[1,2)]

[1)]*Institute for Fusion Studies, The University of Texas, Austin, TX 78712, USA*
[2)]*Department of Physics, The University of Texas, Austin, TX 78712, USA*

(Received 16 December 2009 / Accepted 2 March 2010)

Laser-irradiated microclusters can generate energetic ions that produce fusion reactions. The amount and spectrum of these ions depend on the cluster-size distribution, electron heating mechanism, and cluster expansion dynamics. This paper describes recent physics results pertinent to the items listed. It is shown that the size distribution of large clusters can be determined from absorption measurements in a pump-probe experiment. It is also shown how a laser can create a two-component electron distribution with a hot minority whose energies exceed the ponderomotive potential. The heating rate and the limitations on electron energy are examined. The hot electron component expands with an equal number of ions. A first-principle model is presented that describes ion acceleration by the hot electron pressure together with adiabatic cooling of the hot electrons.

Keywords: laser-cluster interaction, stochastic electron heating, ion acceleration, cluster-size distribution

DOI: 10.1585/pfr.5.S2071

1. Introduction

Laser interactions with a mixture of a gaseous plasma and microclusters exhibit a number of interesting phenomena, including fusion neutron production. Microclusters are generated in laboratory experiments by a supersonic gas jet expanding into a vacuum. Gas condensation produces small liquid density droplets and a high-intensity laser pulse converts them quickly into dense plasmas (microclusters). Neutron yield in laser-cluster experiments [1] results from collisions of fast deuterons (with energies above 10 keV) generated by expanding microclusters. At moderate laser intensities, the average energy absorbed per electron and the ponderomotive potential are well below 10 keV (both are 2.5 keV for the parameters of Ref. [1]), which raises the question about the mechanism of ion acceleration to the energies required for fusion reactions. A plausible resolution of this difficulty is that the laser field creates a two-component electron distribution with a cold majority and a hot minority [2, 3]. In this scenario, the hot minority undergoes stochastic heating, which allows it to reach energies exceeding the ponderomotive potential. The pressure of the hot component forces the cluster to expand, accelerating ions. Since only large clusters can produce sufficiently fast ions, the knowledge of the tail of the cluster-size distribution is essential to interpret the experiments and make quantitative predictions.

In this paper we address all three key ingredients needed to find the population of fast ions generated by expanding clusters: cluster-size distribution, electron heating, and ion acceleration. First we discuss a method for finding the size distribution of large clusters from absorption measurements in a pump-probe experiment with a variable delay between the pulses. We then present a numerical simulation that demonstrates how the two-component electron distribution is formed and how the hot minority is heated stochastically. Finally, we review a first-principle model that describes ion acceleration in an electric field generated by the hot electrons [2].

2. Cluster-size Distribution

The distribution of large clusters over sizes can be recovered from absorption measurements in a pump-probe experiment with a variable delay between the two pulses. This section gives a brief overview of the method and measurements described in detail in Ref. [4].

In our experiments, clusters are formed by condensation in a room temperature pulsed supersonic argon jet located inside a vacuum chamber. A Series-9 pulsed solenoid valve from Parker Hannifin (General Valve division), backed by pressure $P = 41,\ 350$ mbar, opened for 1.5 ms to admit gas into a conical nozzle with orifice diameter $d = 750\,\mu$m and half expansion angle $\alpha = 11^\circ$. For the absorption experiment, a 800 nm, 100 fs pulse from a 10 Hz Ti:sapphire laser system was split into two beams. A pump pulse (400 nm, 100 fs) was generated by frequency doubling one beam in a KDP crystal. The pump pulse had a beam diameter of 40 μm. The other 800 nm beam was used as a probe with a delay controlled by a translation stage. The focused pump intensity is 10^{15} W/cm^2. The probe pulse, focused by a separate lens, had a diameter of approximately 30 μm and intensity of 2×10^{13} W/cm^2. The pump and probe intersect at a small angle of 2°. The energy absorption is determined by measuring the probe

author's e-mail: alexey@mail.utexas.edu

pulse energy with a pyroelectric energy meter.

The measured relative absorption $\kappa(\tau)$ [see Fig. (2)] can be expressed in terms of the refractive index of the medium $n(\tau)$,

$$\kappa(\tau) = 1 - \exp\left(-2\frac{\omega L}{c}\mathrm{Im}\left[n(\tau) - 1\right]\right), \quad (1)$$

where ω is the frequency of the probe pulse, L is the distance traveled by the pulse in the medium, and c is the speed of light. The absorption is dominated by a critical-density resonance in clusters, so that

$$\mathrm{Im}\left[n(\tau) - 1\right] = 2\pi \int_0^\infty \mathrm{Im}\left[\alpha\left(\tau, R_0\right)\right] F(R_0)\mathrm{d}R_0, \quad (2)$$

where $F(R_0)\mathrm{d}R_0$ is the number of clusters per unit volume with initial radii ranging from R_0 to $R_0 + \mathrm{d}R_0$. The function $\alpha(\tau, R_0)$ under the integral is the polarizability of a single cluster. The gaseous plasma contribution to the absorption coefficient is neglected, because this plasma is underdense.

In order to find $\alpha(\tau, R_0)$, we consider: 1) ionization and electron heating by the pump pulse; 2) cluster expansion after the pump pulse; and 3) the response of cluster electrons to the probe pulse. The model for the polarizability presented below describes electrons as isothermal due to their high heat conductivity and it neglects ion expansion during the probe pulse, which is justified for delays longer than the duration of the pulse. Ions are treated as cold.

The ionization begins with the tunnel ionization that quickly generates seed electrons. The collisional ionization caused by thermal electrons then takes over and dominates until the end of the pulse. The pump pulse heats the electrons via inverse bremsstrahlung during electron-ion collisions. The electron-electron collisions keep the electron distribution Maxwellian. We define Z_0 and T_0 as an average ion charge state and electron temperature at the end of the pump pulse. These quantities are insensitive to the cluster radius. We use the ionization and heating rates given in Ref. [5] to find that $T_0 \approx 200\,\mathrm{eV}$ and $Z_0 \approx 9$ for our experimental parameters.

Cluster expansion after the pump pulse is described by the following set of equations:

$$\frac{\partial n_\mathrm{i}}{\partial t} + \frac{1}{r^2}\frac{\partial}{\partial r}\left(v_\mathrm{i} n_\mathrm{i} r^2\right) = 0, \quad (3)$$

$$\frac{\partial v_\mathrm{i}}{\partial t} + v_\mathrm{i}\frac{\partial v_\mathrm{i}}{\partial r} = -\frac{Z_0 T}{m_\mathrm{i} n_\mathrm{i}}\frac{\partial n_\mathrm{i}}{\partial r}, \quad (4)$$

$$T(t) = T_0 - \frac{2}{3Z_0}\left(\int_0^\infty \frac{m_\mathrm{i} v_\mathrm{i}^2}{2} n_\mathrm{i} r^2 \mathrm{d}r\right)\left(\int_0^\infty n_\mathrm{i} r^2 \mathrm{d}r\right)^{-1}, \quad (5)$$

where n_i and v_i are the ion density and velocity and T is the electron temperature. Equations (3) - (5) are the continuity, ion momentum balance, and energy conservation equations, respectively. All clusters are assumed to be spherically symmetric with the same uniform initial density $n_0 = 1.8 \times 10^{22}\,\mathrm{cm}^{-3}$. We solve Eqs. (3) - (5) numerically for a reference cluster with $R_0 = R_*$ to obtain

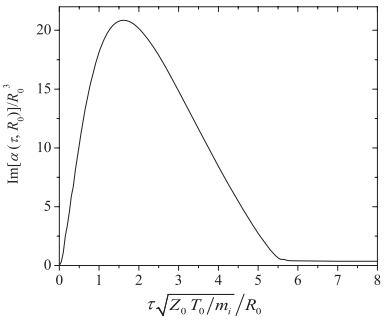

Fig. 1 Normalized polarizability for a single cluster.

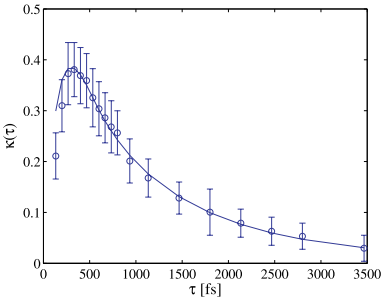

Fig. 2 Measured (open circles) and calculated (solid line) relative absorption as a function of the delay between the pump and the probe.

$n_\mathrm{i}(r, t; R_*)$, $v_\mathrm{i}(r, t; R_*)$, and $T(t; R_*)$. Equations (3) - (5) are invariant with respect to a rescaling transformation $r \to \gamma r$, $t \to \gamma t$. We use this transformation to find the solution for other initial cluster radii.

We follow the procedure used in Ref. [6] to calculate the cluster polarizability for a known electron density profile. Using the rescaling relation for the ion density, we find that the rescaled polarizability is $\alpha(\tau, R_0) = (R_0/R_*)^3\alpha(\tau R_*/R_0, R_*)$. Figure 1 shows $\mathrm{Im}[\alpha(\tau, R_*)]$ for the computed density. The peak is due to the plasma resonance present in a cluster. The cutoff occurs during the expansion when the resonance disappears. The normalized cutoff time is independent of the size, so that the cutoff occurs at longer delays τ for larger clusters.

The key result of our model is that only large clusters contribute to the absorption at long delays. Therefore, their distribution can be recovered by fitting the tail of $\kappa(\tau)$. We achieve a good fit of the absorption data at $\tau \geq 333$ fs (see Fig. 2) using a shifted lognormal distribution,

$$F(R_0) = \frac{c}{4\pi\omega}\frac{1}{La^4}\frac{A/(\sigma\sqrt{2\pi})}{R_0/a - \chi}\exp\left(-\frac{\left[\ln(R_0/a - \chi) - \mu\right]^2}{2\sigma^2}\right), \quad (6)$$

where $A = 1.30$, $\chi = 0.12$, $\mu = -2.64$, $\sigma = 0.89$ and the radius is normalized to $a = 20\,\mathrm{nm}$.

The presented model attributes the entire measured absorption to the plasma resonance in clusters. This requires the electron collision frequency to be lower than the laser frequency, which is indeed the case at the beginning

of cluster expansion. However, the electron cooling during the expansion increases the rate of electron-ion collisions. On the other hand, the energy release via three-body recombination may prevent fast cooling. Our future plan is to quantify the effect of recombination in order to evaluate the role of electron collisions self-consistently.

3. Electron Heating

For sufficiently short laser pulses, electron heating and ion acceleration occur consecutively. Therefore, we first examine electron heating, assuming that the ions are immobile. This approach enables us to identify the key features that would be present in a more complete model.

We consider an ideally conducting slab in an oscillating externally applied electric field, which is perpendicular to the slab. We distinguish two groups of electrons: hot electrons and cold electrons. The conductor freely emits new cold electrons as long as the total electric field points towards the surface. By definition, the cold electrons are those that have never been emitted, whereas the hot electrons are the ones that exit the slab at least once (even if they reenter). The electron motion through the slab is collisionless. There is no electric field inside the slab. Consequently, the electrons move ballistically until reappearing on the opposite side of the slab.

This system is an adequate model of electron dynamics in a large cluster [2], where the hot electrons remain confined by a narrow potential barrier near the cluster surface. In such clusters, the total electric field is normal to the surface and it is proportional to $\cos\theta$, where θ is the polar angle in a spherical system of coordinates with the axis directed along the laser electric field. The hot electrons move predominantly radially and their excursion from the cluster surface is less than the cluster radius. The slab electrons then represent a group of cluster electrons with the same value of θ and $\pi - \theta$.

We simulate the electron dynamics in the slab using a one-dimensional PIC code. The electric field in the vacuum region is calculated by integrating the electron space-charge outside of the slab. If the electric field at the surface of the slab is directed towards the slab, then our solver extracts cold electrons and places them into vacuum next to the surface. The number of extracted electrons at each time step is such that the field on the surface vanishes. The electrons in the vacuum region follow the equations of motion with a self-consistent electric field. Once electrons reenter the slab, the code computes the time of flight through the slab and emits these electrons on the opposite side at the corresponding time instant.

The applied electric field is $E = E_0 \sin(\omega t)$. The only dimensionless parameter in the problem is

$$\chi \equiv \frac{m_e \omega^2 L}{|e|E_0}, \tag{7}$$

where L is the width of the slab. The electrons emitted into the vacuum are pushed back when the direction of the applied electric field reverses. The energy of the returning electrons is on the order of the ponderomotive energy $\frac{1}{2}m_e(|e|E_0/m_e\omega)^2$. This process is known as vacuum heating [7]. The vacuum heating leads to an increase in the number of hot electrons, as the returning electrons are replaced by newly emitted cold electrons during the next period of the applied filed. The emission of cold electrons continues until the first generation of the hot electrons traverses the slab.

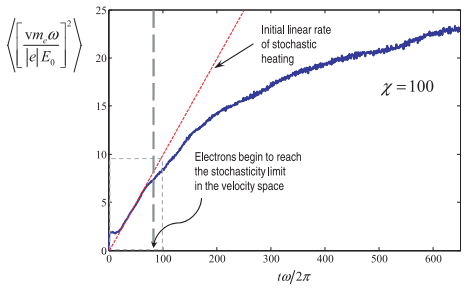

Fig. 3 Time-dependence of the average hot electron energy. Here v is the electron velocity and the angular brackets denote the averaging over the hot electron population.

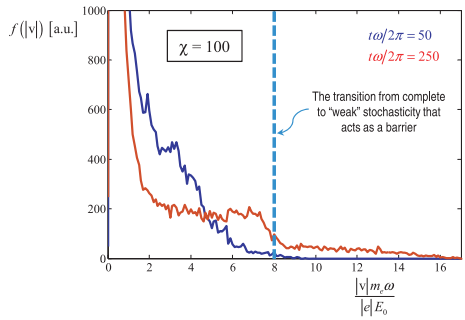

Fig. 4 Velocity distribution function $f(|v|)$ of hot electrons inside the slab at $t\omega/2\pi = 50$ and $t\omega/2\pi = 250$.

If $\chi \gg 1$, then it takes several field periods for the first generation of electrons to traverse the slab. This allows for the dephasing between the electron velocity and the total field to occur. The electron interaction with the total field then becomes stochastic. This process is analogous to the Fermi heating [8], but in our case the problem is more complicated because of the dependence of the total field on the electron energy distribution. The average energy of the hot electron population is shown as a function of time in Fig. 3 for $\chi = 100$. The initial flat segment at $t < 10\, t\omega/2\pi$ corresponds to the vacuum heating. The energy grows because of the stochastic heating and the initial growth rate is linear.

The hot electron distribution function inside the slab is shown in Fig. 4. At $\omega t/2\pi = 50$, the distribution has a well pronounced flat region below $v_* \approx 8|e|E_0/m_e\omega$. The "barrier" in the velocity space at $v = v_*$ results from the loss of stochasticity. The value of v_* is determined by the Chirikov resonance-overlap criterion and it is proportional to $\sqrt{L}$. Once first hot electrons reach the "barrier" in the

velocity space, the heating slows down from the initial linear rate (see Fig. 3).

The described picture shows how the applied field generates a hot electron population. These electrons undergo stochastic heating, which can increase their energy significantly compared to the ponderomotive potential.

4. Ion Acceleration

In a spherical cluster, the heating mechanism of Sec. 3 generates hot electrons with predominantly radial velocities. In order to obtain a simple qualitative picture of cluster expansion and ion acceleration, we assume that the electron density is spherically symmetric. Reference [9] presents an analytical solution for this case for a cluster with a uniform ion background, uniform cold electron core, and a small population of hot electrons. In what follows, we summarize the results of Ref. [9].

Prior to the expansion, the cold and hot electron populations occupy the same volume. Only the hot electron cloud expands, which causes a breakdown of quasineutrality at the edge of the cold electron core in the form of a double layer. The cold electron core is a volume with cold electrons, hot electrons, and ions. The core maintains its shape to stay neutral and keep the total electric field inside equal to zero. The ions are continuously extracted from inside the core where their density significantly exceeds the hot electron density. This explains why a double layer forms and persists at the cold core boundary during the expansion. The structure of the double layer is shown in Fig. 5. The double layer produces a quasineutral supersonic plasma flow. Since the flow is supersonic, its density profile has two distinct regions: a quasi-static region adjacent to the double layer and a rarefaction wave associated with the expanding edge of the plasma. The electron motion is collisionless, so that sufficiently fast electrons are able to reach the rarefaction wave. The time-dependent electric field at the edge reflects these electrons back and, in the process, they lose some of their energy. The result of the cooling down is the decrease in the potential difference between the cold electron core and the rarefaction wave. This process continues until all hot electrons cool down and transfer their energy to the ions in the quasineutral expanding flow. The resulting ion spectrum is shown in Fig. 6. It has been calculated for a top-hat initial velocity distribution of hot electrons (the corresponding energy distribution is shown on the same figure) [9]. We draw the following qualitative conclusions from the solution. The average ion energy gain is of the order of the hot electron energy before the expansion. There is also a considerable fraction of fast ions whose maximum energy exceeds the initial maximum electron energy. The ions gain as much as 50% of their final energy moving through the double layer. However, the fastest ions result from an additional significant acceleration in the rarefaction wave.

The neutron yield is sensitive to the details of the tail

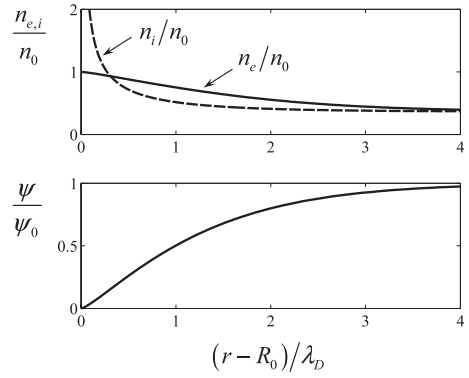

Fig. 5 Electron and ion density profiles (n_e and n_i) and electrostatic potential (ψ) in the double layer. The densities are normalized to the hot electron density n_0 at the surface of the cold electron core, located at $r = R_0$. The electrostatic potential is normalized to its value at the double layer exit $\psi_0 = -\sqrt{3\mathcal{E}_H/2|e|}$, where $\mathcal{E}_H$ is the maximum (cutoff) electron energy. The radial scale is normalized to $\lambda_D = \mathcal{E}_H/4\pi n_0 e^2[\mathcal{E}_H^{t=0}/\mathcal{E}_H]^{1/4}$.

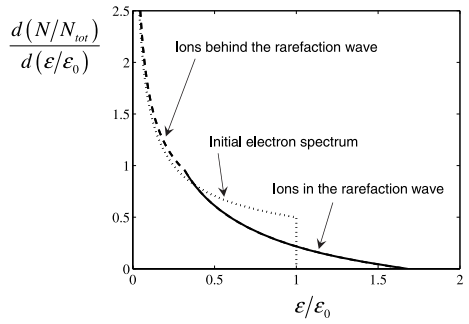

Fig. 6 Asymptotic ion energy spectrum (solid and dashed curves) and initial hot electron energy spectrum (dotted curve). Kinetic energies of ions and electrons are normalized to $\mathcal{E}_H^{t=0}$. The number of particles is normalized to the total number of hot electrons N_{tot}.

of the ion spectrum. Therefore, a self-consistent numerical simulation that incorporates all three elements considered in this paper (cluster-size distribution, electron heating mechanism, and cluster expansion dynamics) is required to make a quantitative prediction regarding the neutron yield.

Acknowledgments

This work was supported in part by the U.S. Department of Energy under Contracts No. DE-FC52-08NA-28512, DE-FG02-04ER-54742, and DE-FG03-96ER-40954.

[1] T. Ditmire, J. Zweiback, V. P. Yanovsky, T. E. Cowan, G. Hays and K. B. Wharton, Nature (London) **398**, 489 (1999).
[2] B. N. Breizman, A. V. Arefiev and M. V. Fomyts'kyi, Phys. Plasmas **12**, 056706 (2005).
[3] B. N. Breizman and A. V. Arefiev, Plasma Phys. Rep. **29**, 593 (2003).

[4] A. V. Arefiev, X. Gao, M. R. Tushentsov *et al.*, High Energy Density Physics **6**, 121 (2009) published online: 13 January 2010, doi:10.1016/j.hedp.2009.12.010.
[5] T. Ditmire, T. Donnelly, A. M. Rubenchik *et al.*, Phys. Rev. A **53**, 3379 (1996).
[6] H. M. Milchberg, S. J. McNaught and E. Parra, Phys. Rev. E. **64**, 056402 (2001).
[7] F. Brunel, Phys. Rev. Lett. **59**, 52 (1987).
[8] M. A. Lieberman, "The Dynamics of Fermi Acceleration" in *Electron Kinetics and Applications of Glow Discharges*, doi:10.1007/b115089.
[9] B. N. Breizman and A. V. Arefiev, Phys. Plasmas **14**, 073105 (2007).